



Synthesis and correlation between structure and photovoltaic performance of two-dimensional BDT-TPD polymers



Nam Jeong Hong^{a,1}, Hanok Park^{b,1}, Myoung-Jin Baek^b, Soo-Hyoung Lee^b, Jo Jeong^a, Jun Hui Park^{a,**}, Kyukwan Zong^{a,*}

^a Department of Chemistry Education, Div. of Science Education, Chonbuk National University, 567 Baekje-ro, Jeonju 561-756, Republic of Korea

^b Department of Chemical Engineering, Chonbuk National University, 567 Baekje-ro, Jeonju 561-756, Republic of Korea

ARTICLE INFO

Article history:

Received 21 March 2016
Received in revised form
4 May 2016
Accepted 5 May 2016
Available online 20 May 2016

Keywords:

Polymer solar cells
BDT-TPD polymers
Two-dimensional structure
PCE

ABSTRACT

Four BDT-TPD polymers (**PA–PD**) were synthesized by modifying the alkylthienyl chains on BDT, placing spacer group between BDT and TPD, and installing extended conjugated side chains on the BDT of the polymer to investigate the correlation between structure and photovoltaic performance for these polymers. The molecular weight of **PA–PD** polymers ranged from the highest ($M_n = 80$ kDa for **PA**) to the lowest ($M_n = 7.9$ kDa for **PD**), and their decomposition temperatures at 5% weight loss were in the range 401–435 °C. **PA**, **PB**, and **PC** showed similar UV–vis absorption spectra; however, **PD** showed much broader absorption spectrum in the entire UV–vis region, because of the extended conjugated side chains. The HOMO levels of the polymers were -5.72 , -5.63 , -5.48 , and -5.61 eV for **PA**, **PB**, **PC**, and **PD**, respectively, indicating very low-lying HOMO energy levels. The bandgaps of these polymers were calculated and found to be in the range 1.85–1.88 eV. The theoretical calculations clearly show that the torsional angles between the alkylthienyl group and BDT unit of the simplified dimer correlated to the π -orbital delocalization, suggesting that the HOMO π -electrons of vertically aligned conjugated side chains do not delocalize well in the polymers such as **PA**, **PB**, and **PC** bearing high torsional angles. The optimized weight ratios of the polymer to PC₆₁BM were determined to be 1:1, 1:1.5, and 1:1 for **PA**, **PC**, and **PD**, respectively, and the average PCEs of the devices were 5.36%, 4.62%, and 2.74% for **PA**, **PC**, and **PD**, respectively, after optimization with 1,8-diiodooctane (DIO). A relatively small amount of DIO as an additive was necessary to reach the optimal PCEs of the devices, and the device incorporating PC needed only 0.5% DIO to obtain the best PCE. The AFM study reveals that the blend films after adding DIO showed much smooth morphologies, and the blend film of **PA** exhibited more crystalline property, as shown by the XRD analysis.

© 2016 Elsevier B.V. All rights reserved.

1. Introduction

Polymer solar cells (PSCs) have recently received significant attention as renewable energy sources owing to their potential in fabricating large-area, flexible, and cost effective solar panels by roll to roll printing process [1–4]. Donor–acceptor conjugated copolymers have been widely used in high-performance organic electronic devices. When the polymers are prepared by careful selection of the donor and the acceptor units, they may offer

excellent control of the electronic bandgap, resulting in tunable light absorption for organic photovoltaic. Conjugated polymers incorporating alternating donor and acceptor units provide relatively low bandgaps, probably because of the introduction of intermolecular charge transfer complexes, and these low bandgap polymers are considered as promising candidates for highly efficient photovoltaic benefited with a broad range of absorption up to near IR region [5–7]. To design high efficiency photovoltaic polymers, understanding the correlation between the molecular structures and photovoltaic properties of the conjugated polymers is of critical importance. Recently, several methods were proposed to improve the photovoltaic properties of conjugated polymers by using π -spacers or conjugated side chains, and these studies have provided valuable guidelines for the design of conjugated molecular structure [8–10]. Recently, benzo[1,2-b:4,5-b']

* Corresponding author.

** Corresponding author.

E-mail addresses: echem@jbnu.ac.kr (J.H. Park), kzong@jbnu.ac.kr (K. Zong).

¹ These authors are equally contributed to this work.

dithiophene–thieno[3,4-c]pyrrolo-4,6-dione (BDT-TPD) polymers applied for PSCs have received significant attention owing to their extraordinary high open circuit voltage (V_{oc}) values, which are crucial for achieving high power conversion efficiency (PCE) values of PSCs. Several research groups reported the PCE, V_{oc} , short circuit current density (J_{sc}), and fill factor (FF) values of 4.2–6.6%, 0.85–0.91 V, 9.1–11.5 mA cm⁻², 0.51–0.68, respectively, for the PSCs based on PBDDT-TPD [11–14]. Replacing the O-alkoxy groups by the alkylthienyl groups on BDT unit significantly improved the thermal stabilities and V_{oc} (up to 1 V) of PSCs [15–17]. More recently, replacing the alkylthienyl groups with more extended conjugated side chains on the BDT units of the polymers significantly enhanced PCEs not only of the BDT-TPD polymers [18], but also of other polymers by significantly improving the optical absorption in the range 300–500 nm [19,20]. Therefore, investigating the correlation between structure and photovoltaic performance of BDT-TPD polymers is of great interest to us to find the room to further improve PCEs of BDT-TPD polymers by structural engineering and then designing new polymers based on BDT-TPD structure with high PCE. In this study as illustrated in Fig. 1, we designed and synthesized four BDT-TPD polymers based on alkyl group engineering on the BDTT unit, spacer engineering between the donor and acceptor units of the polymer backbone, and side chain engineering on the BDT unit. The correlation between the structural and photovoltaic property of these polymers were comprehensively studied, and the results provide thoughtful insight for improving the performance of PSCs and designing new polymers based on BDT-TPD for developing better performing PSCs.

2. Experimental

2.1. 5-(2-ethylhexyl)-2-ethynylthiophene (D)

A solution of 2-ethylhexylthiophene (25.24 g, 0.1 mol) in dry THF (50 mL) was cooled to -78°C under argon, and *n*-BuLi (62 mL, 0.11 mol, 2.5 M in hexane) was slowly added to the solution. The reaction mixture was warmed to 50°C and stirred for 2 h. Then, the solution was again cooled to -78°C , followed by adding a solution of I_2 in 50 mL dry THF. The reaction mixture was allowed to warm to

ambient temperature and stirred for 2 h. The reaction mixture was quenched with saturated NH_4Cl and extracted with ether (3×30 mL). The combined organic extract was washed with water, brine, and dried over anhydrous MgSO_4 . After filtering off MgSO_4 , the supernatant was evaporated by rotary evaporator and further concentrated under high vacuum. The crude product was used in the next step without further purification. To a solution of 2-(2-ethylhexyl)-5-iodothiophene (3.2 g, 10 mmol) in diisopropylamine (50 mL) was added CuI (95 mg, 0.5 mmol) and $\text{Pd}(\text{PPh}_3)_2\text{Cl}_2$ (350 mg, 0.5 mmol) at room temperature. The reaction mixture was stirred for 20 h at room temperature and refluxed for 2 h. The reaction mixture was allowed to warm to ambient temperature, quenched with 1 M HCl, and extracted thrice with ether. The combined organic extract were washed with water, brine, and dried over anhydrous MgSO_4 . After filtering MgSO_4 , the filtrate was concentrated by rotary evaporation, and the residue was dissolved in 2 M methanolic NaOH solution to remove TMS and stirred for 10 min. The reaction mixture was quenched with water and extracted with ether (3×30 mL). The product was isolated by column chromatography on silica gel using hexane as the eluent. Pale yellow oil; (60%); ^1H NMR (400 MHz, CDCl_3 , δ): 0.87–0.89 (m, 6H), 11.33 (m, 8H), 1.55 (t, $J = 5.8$, 1H), 2.73 (dd, $J = 6.8$ Hz, 2H), 3.27 (s, 1H) 6.60 (d, $J = 3.9$ Hz, 1H) 7.08 (d, $J = 3.4$ Hz 1H); ^{13}C NMR (100 MHz, CDCl_3 , δ): 10.77, 14.07, 22.94, 25.46, 28.79, 32.28, 34.05, 41.38, 77.46, 80.39, 119.38, 124.94, 132.99, 147.15. Anal. Calcd. for $\text{C}_{14}\text{H}_{20}\text{S}$: C, 76.30; H, 9.15; S, 14.55. Found: C, 76.28; H, 9.16; S, 14.50.

2.2. General procedure for preparation of compound 2

A solution of 2-(2-ethylhexyl)thiophene (11.78 g, 60 mmol) in dry THF was slowly treated with *n*-BuLi (24 mL, 60 mmol, 2.5 M in hexane) at -78°C . The reaction mixture was allowed to warm to 50°C and then stirred for 2 h. To the solution was added 4,8-dihydrobenzodithiophen-4,8-dione (3.3 g, 15 mmol) at 50°C and further stirred for 2 h. The reaction was cooled down to room temperature, followed by the addition of $\text{SnCl}_2 \cdot \text{H}_2\text{O}$ (27 g, 0.12 mol) dissolved in 10% HCl (48 mL) and further stirred for 2 h at room temperature. Ice water was poured into the reaction and extracted with CH_2Cl_2 (3×30 mL). The combined organic extract was washed

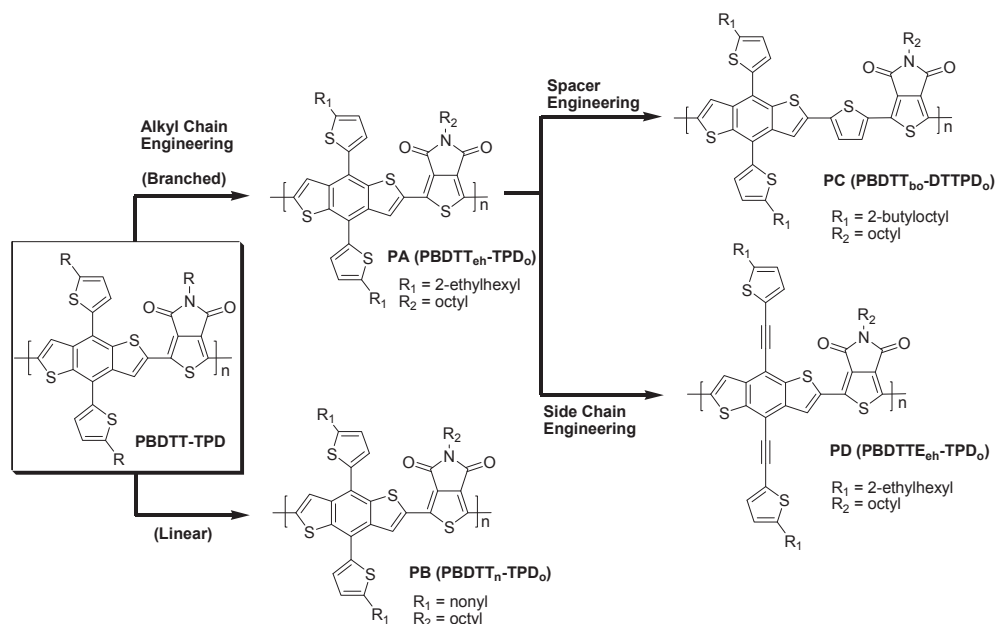


Fig. 1. Schematic illustration for polymer structure engineering carried out in this study.

with water, followed by brine, and then dried over anhydrous MgSO₄. After filtering off MgSO₄, the solution was concentrated under reduced pressure, and the residue was isolated by column chromatography on silica gel.

2.3. 4,8-Bis(5-(2-ethylhexyl)thiophen-2-yl)benzo[1,2-b:4,5-b']dithiophene (2A)

Pale yellow oil; 76% yield; ¹H NMR (400 MHz, CDCl₃, δ): 7.64 (d, 2H), 7.45 (d, 2H), 7.29 (d, 2H) 6.89 (d, 2H), 2.86 (d, 4H), 1.75 (m, 2H), 1.53–1.18 (m, 16H), 0.92–0.83 (m, 12H). ¹³C NMR (300 MHz, CDCl₃, ppm) δ: 145.84, 139.11, 137.34, 136.62, 127.83, 127.58, 125.50, 124.20, 123.56, 41.60, 34.38, 32.61, 29.05, 25.84, 23.17, 14.32, 11.06. Anal. Calcd. for C₃₄H₄₂S₄: C, 70.53; H, 7.31; S, 22.15. Found: C, 70.50; H, 7.25; S, 22.11.

2.4. 4,8-Bis(5-(2-nonyl)thiophen-2-yl)benzo[1,2-b:4,5-b']dithiophene (2B)

Yellow powder; 70.6% yield; ¹H NMR (400 MHz, CDCl₃, δ): 0.82 (t, *J* = 6.6 Hz, 3H), 1.22–1.37 (m, 14H), 2.84 (t, *J* = 7.41 Hz, 2H), 6.83 (d, *J* = 3.9 Hz, 1H), 7.22 (d, *J* = 3.9 Hz, 1H), 7.38 (d, *J* = 5.8 Hz, 1H) 7.57(d, *J* = 5.8 Hz 1H); ¹³C NMR (100 MHz, CDCl₃, δ): 14.12, 22.69, 29.24, 29.30, 29.38, 29.53, 30.26, 31.62, 31.89, 123.42, 124.07, 124.25, 127.42, 127.76, 136.52, 136.97, 138.99, 147.16; HRMS (FAB) *m/z* Calc. for C₃₆H₄₆S₄: 606.2482, found: 606.2476.

2.5. 4,8-Bis(5-(2-butyloctyl)thiophen-2-yl)benzo[1,2-b:4,5-b']dithiophene (2C)

Light brown oil; 84% yield; ¹H NMR (400 MHz, CDCl₃, δ): 0.84–0.97 (m, 6H), 1.29–1.34 (m, 16H), 1.72 (m, 1H), 2.84 (d, *J* = 6.8 Hz, 2H), 6.87 (d, *J* = 3.41 Hz, 1H), 7.28 (d, *J* = 3.41 Hz, 1H) 7.44(d, *J* = 5.8 Hz 1H) 7.63 (d, *J* = 5.8 Hz 1H); ¹³C NMR (100 MHz, CDCl₃, δ): 14.13, 22.69, 23.01, 26.65, 28.91, 29.66, 31.58, 31.89, 33.07, 33.40, 34.69, 40.02, 123.39, 124.09, 125.36, 127.42, 127.68, 136.52, 137.20, 139.01, 145.72; HRMS (FAB) *m/z* Calc. for C₄₂H₅₈S₄: 690.3421, found: 690.3425.

2.6. 4,8-di(5-(2-ethylhexyl)thiophene-2-ylethynyl)benzo[1,2-b:4,5-b']dithiophene (2D)

Light brown oil; 60% yield; ¹H NMR (400 MHz, CDCl₃, δ): 0.86–0.97 (m, 6H), 1.26–1.42 (m, 8H), 1.61 (t, *J* = 5.8 Hz, 1H), 2.78 (d, *J* = 6.3 Hz, 2H), 6.72 (d, *J* = 3.4 Hz, 1H) 7.25 (d, *J* = 1.7 Hz, 1H) 7.56(d, *J* = 5.3 Hz 1H) 7.66 (d, *J* = 5.3 Hz, 1H); ¹³C NMR (100 MHz, CDCl₃, δ): 10.83, 14.12, 22.98, 25.53, 28.86, 32.37, 34.28, 41.51, 88.76, 92.98, 111.80, 120.13, 123.20, 125.55, 128.06, 132.65, 137.97, 139.95, 148.20; HRMS (FAB) *m/z* Calc. for C₃₈H₄₂S₄: 626.2169, found: 626.2171.

2.7. General procedure for preparation of compound 3

To a solution of 4,8-bis(5-(2-ethylhexyl)thiophene-2-yl)benzo[1,2-b:4,5-b']dithiophene (2A, 3.4 g, 5.9 mmol) in dry THF was added *n*-BuLi (5.9 mL, 14.75 mmol, 2.5 M in hexane) at –78 °C. The reaction was stirred for 1 h at –78 °C and for 0.5 h at room temperature. Then, the reaction was cooled to –78 °C and treated with a solution of trimethyltinchloride (3.53 g, 17.7 mmol) via a syringe. Water (50 mL) was poured into the reaction and extracted with ethyl acetate (3 × 30 mL). The combined organic extract was washed with water, followed by brine and dried over anhydrous MgSO₄. After concentrating under reduced pressure, the residue was recrystallized from ethyl acetate/methanol.

2.8. 2,6-Bis(trimethyltin)-4,8-di(5-(2-ethylhexyl)thiophen-2-yl)benzo[1,2-b:4,5-b']dithiophene (3A)

Yellow crystal; 66% yield. Known compound and also see the reference [23].

Anal. Calc. for C₄₀H₅₈S₄Sn₂: C, 53.11; H, 6.46; S, 14.18; Sn, 26.25; Found: C, 53.49; H, 6.48, S, 14.58; Sn, 25.45.

2.9. 2,6-Bis(trimethyltin)-4,8-di(5-(2-nonyl)thiophen-2-yl)benzo[1,2-b:4,5-b']dithiophene (10B)

Yellow crystals; 64.3%; ¹H NMR (400 MHz, CDCl₃, δ): 0.39(t, *J* = 28.2 Hz 9H), 0.88 (t, *J* = 6.83 Hz, 3H), 1.27–1.45 (m, 12H), 1.75–1.83 (m, 2H), 2.92 (t, *J* = 7.8 Hz, 2H), 6.92 (d, *J* = 3.4 Hz, 1H) 7.31(d, *J* = 3.4 Hz 1H) 7.69 (t, *J* = 15.1 Hz, 1H); ¹³C NMR (100 MHz, CDCl₃, δ): 14.12, 22.69, 29.32, 29.43, 29.57, 30.28, 31.57, 31.90, 122.39, 124.15, 127.61, 131.01, 131.15, 137.31, 137.74, 142.22, 143.27, 146.78. Anal. Calc. for C₄₂H₆₂S₄Sn₂: C, 54.19; H, 6.70; S, 13.75, S, 25.46, found: C, 54.29; H, 6.67, S, 14.36; Sn, 24.68.

2.10. 2,6-Bis(trimethyltin)-4,8-di(5-(2-butyloctyl)thiophen-2-yl)benzo[1,2-b:4,5-b']dithiophene (10C)

Light brown oil (the product was purified by passing through activated charcoal pad, because trimethyltin group was too labile to survive against chromatography on silica gel or alumina). 70.6% yield; ¹H NMR (400 MHz, CDCl₃, δ): 0.39 (s, 9H), 0.88–0.91 (m, 6H), 1.29–1.37 (m, 16H), 2.04 (s, 1H), 2.86 (d, *J* = 6.34 Hz, 2H), 6.89 (d, *J* = 3.41 Hz, 1H) 7.31 (d, *J* = 3.41 Hz 1H) 7.68 (s, 1H); ¹³C NMR (100 MHz, CDCl₃, δ): 14.13, 14.17, 22.68, 23.03, 26.54, 26.69, 28.93, 29.68, 31.90, 33.05, 33.47, 34.71, 40.01, 60.37, 122.40, 125.28, 126.39, 127.51, 131.12, 137.29, 137.96, 142.20, 143.27, 145.33; FAB-HR *m/z* Calc. for C₄₈H₇₄S₄Sn₂: 1018.2717, found: 1018.2724.

2.11. 2,6-Bis(trimethyltin)-4,8-di(5-(2-ethylhexyl)thiophene-2-ylethynyl)benzo[1,2-b:4,5-b']dithiophene (10D)

Yellow powder; 47% yield; ¹H NMR (400 MHz, CDCl₃, δ): 0.47 (t, *J* = 0.9 Hz, 9H), 0.89–0.91 (m, 6H), 1.31–1.39 (m, 8H), 1.54 (s, 1H), 2.78 (d, *J* = 6.8 Hz, 2H), 6.73 (d, *J* = 3.9 Hz, 1H) 7.27 (d, *J* = 3.4 Hz, 1H) 7.68 (t, *J* = 14.1 Hz, 1H); ¹³C NMR (100 MHz, CDCl₃, δ): 10.83, 14.12, 22.99, 25.54, 28.86, 32.38, 34.30, 41.52, 89.38, 92.26, 109.94, 120.49, 125.48, 130.87, 132.51, 138.83, 143.49, 144.36, 147.90. Anal. Calcd. for C₄₄H₅₈S₄Sn₂: C, 55.48; H, 6.14; S, 13.46; Sn, 24.92; Found: C, 55.38; H, 6.12; S, 15.24; Sn, 23.26.

2.12. Typical procedure of the preparation of PBDTT_{eh}-TPD_o

BDDTeh (400 mg, 0.442 mmol), TPDoct-diBr₂ (187 mg, 0.442 mmol), Pd₂(dba)₃ (6.07 mg, 1.5 mol%), and p(*o*-tolyl)₃ (4 mg, 3 mol%) were added to a 50 mL schlenk tube and evacuated and backfilled with argon four times. Toluene (10 mL, degassed by 4 freeze/pump/thaw cycles) was then added, and the reaction mixture was heated to 110 °C and stirred for 3 days. The reaction mixture was then cooled to 50 °C, and the large spatula tip of diethylammoniumdiethyldithiocarbamate and 10 mL toluene was added and stirred for 1 h. The mixture was then pipetted into 300 mL methanol, precipitating the polymer, and this was filtered into a cellulose thimble and purified by soxhlet extraction with methanol (1 day), acetone (1 day), hexane (1 day), dichloromethane (1 day), and chloroform (3 h). Chloroform soluble fraction was added to 300 mL methanol, and the solid was collected by passing through a 20 μm pore size nylon filter paper.

2.13. PA (PBDTTe_{eh}-TPD_o)

Dark brown solid (lustrous when filmed); 278 mg (75% yield); GPC: $M_n = 80,455$, $M_w = 151,310$, PDI = 1.88. Anal. Calc. for C₅₀H₆₃NO₂S₅: C, 69.0; H, 7.30; N, 1.61; S, 18.42, found: C 68.33; H, 7.19; N, 1.65; S, 20.73.

2.14. PB (PBDTTe_n-TPD_o)

Dark brown solid (lustrous and porous when filmed); 285 mg (77% yield). GPC: $M_n = 52,243$, $M_w = 84,915$, PDI = 1.627. Anal. Calc. for C₅₀H₆₁NO₂S₅: C, 69.16; H, 7.08; N, 1.61; S, 18.46, found: C, 68.7; H, 6.98; N, 1.71; S, 17.78.

2.15. PC (PBDTTe_{bo}-TPD_o)

Dark brown solid (lustrous when filmed); 190 mg (55% yield). GPC: $M_n = 24,915$, $M_w = 54,715$, PDI = 2.196. Anal. Calc. for C₆₆H₈₃NO₂S₇: C, 69.12; H, 7.2; N, 1.22; S, 19.57, found: C, 69.12; H, 7.21; N, 1.3; S, 18.88.

2.16. PD (PBDTTe_{eh}-TPD_o)

A dark brown solid, 185 mg (45% yield). GPC: $M_n = 7557$, $M_w = 15,747$, PDI = 2.084. Anal. Calc. for C₅₄H₆₃NO₂S₅: C, 70.62; H, 6.91; N, 1.53; S, 17.46, found: C, 69.89; H, 6.54; N, 1.50; S, 19.50.

3. Results and discussion

3.1. Synthesis and characterization of the polymers

The synthetic routes for monomers and polymers are shown in Scheme 1. The detailed experimental procedures for the monomers and polymers are given in the Experimental Section. BDT monomers, 3A–D, were synthesized according to reported methods [16,21–23]. Especially, for the synthesis of 3D as a new side chain, D was synthesized from A through two steps, iodination at the 5-position of 2-(2-ethylhexyl)thiophene and ethynylation of A-1 under the Sonogashira reaction condition. These four polymers were prepared by employing the Stille coupling reaction with tris(dibenzylideneacetone)dipalladium (Pd₂dba₃) and tri(*o*-tolyl) phosphine (P(*o*-tol)₃) as catalysts [16]. All the polymers showed good solubility in chloroform, chlorobenzene, and 1,2-dichlorobenzene at ambient temperature except PB. Gel permeation chromatography (GPC) using monodispersed polystyrene as the standard and chloroform as the eluent was used to measure the number-average molecular weights (M_n) and polydispersity index (PDI) of the polymers (Table 1). M_n of the polymers are as follows: PA (PBDTTe_{eh}-TPD_o), 80.4 KDa (PDI = 1.88); PB (PBDTTe_n-TPD_o), 52.2 KDa (PDI = 1.63); PC (PBDTTe_{bo}-TPD_o), 24.9 KDa (PDI = 2.19); and PD (PBDTTe_{eh}-TPD_o), 7.6 KDa (PDI = 2.08). Notably, PA exhibited noticeably high molecular weight with a reasonable PDI (1.88), which is considered to be highly promising for the device stability.

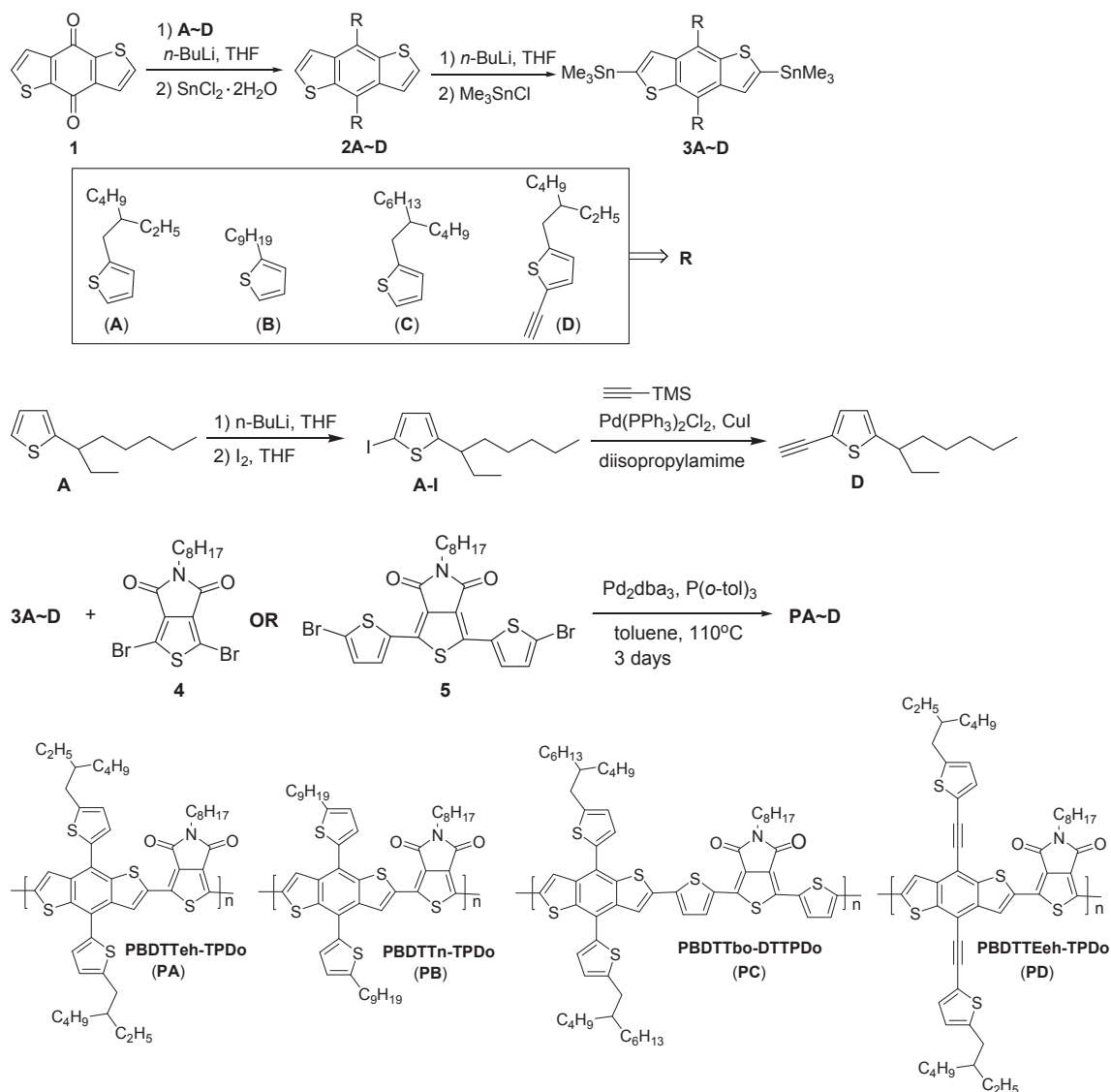
The thermal stability of the polymers was evaluated by thermogravimetric analysis (TGA), and the plot is shown in Fig. 2. The thermal decomposition temperature (5% weight loss) of PA, PB, PC, and PD were 435, 434, 401, and 413 °C, respectively. The thermal stabilities of PA and PB having high molecular weight appeared to be enhanced in comparison with those of PC and PD. This result indicates that the polymers are thermally stable enough for photovoltaic applications.

3.2. Optical properties

The optical properties of the polymers, PA–PD were investigated by UV–vis absorption spectroscopy in dilute chloroform solutions and as thin films. The detailed absorption data are listed in Table 2. Fig. 3 shows absorption spectra of PA in solution and as thin film. Although the λ_{max} in solution is consistent with the previous report, λ_{max} as thin film is 7 nm more red-shifted than that reported previously [16]. The absorption spectra of PB installed with linear alkyl chains are shown in Fig. 3. No significant bathochromic shift was observed on going from solution to the solid state, suggesting that strong aggregation of this polymer in solution is promoted by more orderly layered polymers with linear alkyl chain. Another distinct characteristic of the spectrum from PB compared to that of PA is that a shoulder peak next to the absorption maximum becomes much pronounced in solution and is also consistent with the findings reported previously [16]. The structural variation in the polymer by placing a spacer between donor and acceptor units (PC) dramatically changed the absorption spectra, whereas the shoulder of PA and PB became the absorption maximum in PC. Similarly as shown in PB, no significant bathochromic shift was observed between in solution and as thin film, suggesting that a high degree of macromolecular ordering is favored even in dilute solution. The UV–vis spectrum of PD exhibited two λ_{max} at 367 and 563 nm and a shoulder peak at 625 nm. The absorption maximum at the shorter wavelength (367 nm) may attribute to the BDT unit bearing conjugated thienylethynyl side chain and is approximately consistent with the previous report [18]. Two peaks at 563 and 625 nm may attribute to the intramolecular charge transfer (ICT) between the acceptor (TPD) and the donor (BDT) units [24].

3.3. Electrochemical properties

Cyclic voltammetry (CV) was used to investigate the electrochemical properties of the polymers. The HOMO of the polymers was measured by anodic sweep to +1.5 V vs. Fc/Fc⁺. The LUMO energy levels of the polymers were calculated based on the correlation between the optical band gap from the absorption spectra (film) and the HOMO level ($E_{LUMO} = E_{HOMO} + E_g$). It should be noted that the obtained E_{LUMO} is an approximated value because the optical bandgap used as E_g in our calculation neglects the exciton binding energy [25]. The CV curves and the energy levels of the polymers PA–PD are shown in Fig. 4. As shown in Fig. 4a, the CV plots of p-doping process are provided, and they were measured using a Pt disk electrode in the presence of 100 mM TBAPF₆ in acetonitrile at a scan rate of 100 mV/s. The onset oxidation potentials (Φ_{ox}) of PA, PB, PC, and PD were 0.92, 0.83, 0.68, and 0.81 eV, respectively. The HOMO energy levels of the polymer solutions were calculated by assuming the HOMO energy for the Fc/Fc⁺ standard of 4.8 eV with respect to the zero vacuum level. The relation is expressed as follows: $E_{HOMO} = -(\Phi_{ox} + 4.8)$ eV, where Φ_{ox} is the onset oxidation potential relative to the ferrocene external standard [17]. According to the equation, the HOMO levels of the polymers were calculated to -5.72, -5.63, -5.48, and -5.61 eV for PA, PB, PC, and PD, respectively, and are included in the energy level diagram in Fig. 4b. The trend of low-lying HOMO energy levels related to the BDT-TPD polymers well matched with the previous works [16]. Interestingly, the HOMO energy level of -5.72 eV for PA turned out even lower than that (-5.61 eV) reported previously, suggesting that the difference of -0.11 eV of HOMO energy level is considered to be further beneficial for achieving higher V_{oc} in PSCs. To the best of our knowledge, the HOMO energy level of -5.72 eV is the lowest one among the BDT-TPD polymers. Notably, the addition of a spacer between the BDT and TPD unit as exemplified by PC increased the HOMO level significantly (-5.72 eV → -5.48 eV),



Scheme 1. Synthetic routes for the proposed monomers and polymers and the structures of the synthesized polymers.

Table 1
Polymerization results and thermal properties.

Copolymers	Yields (%)	M_n (kDa) ^a	M_w (kDa) ^a	PDI	T_d ($^\circ\text{C}$) ^b
PA	75	80.4	151.3	1.88	435
PB	77	52.2	84.9	1.63	434
PC	55	24.9	54.7	2.19	401
PD	45	7.6	15.7	2.08	413

^a From gel permeation chromatography.

^b From thermogravimetric analysis.

whereas the bandgap almost remained unchanged, supporting that decreasing the electron-deficiency of the polymer by inserting a donor spacer can increase the HOMO energy level of the polymer. More interestingly, **PD** bearing extended conjugated side chains was found to have low-lying HOMO energy level (-5.61 eV), which is considered as a valuable insight for designing 2-D polymers for highly efficient PSCs.

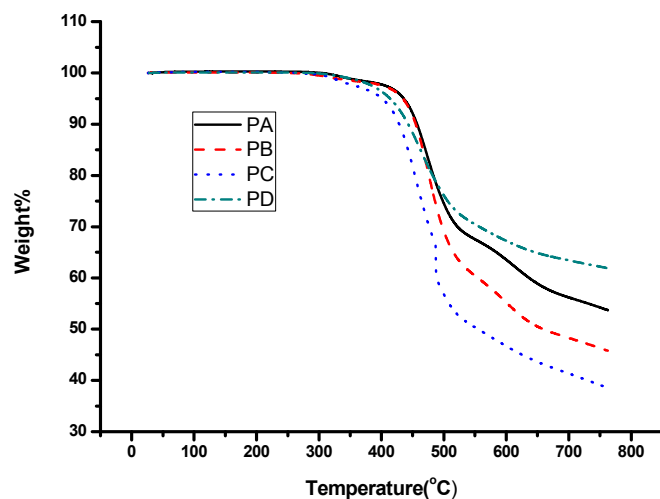


Fig. 2. TGA plots of **PA**, **PB**, **PC**, and **PD**.

Table 2
Optical and electrochemical properties of the polymers.

Polymers	UV–vis								Cyclic voltammetry	
	Solution ^a				Film				$E_{\text{onset}}^{\text{ox}}$ (V)	$E_{\text{HOMO}}^{\text{f}}$ (eV)
	λ_{max} (nm)	λ_{onset} (nm)	E_g^{b} (eV)	$E_{\text{LUMO}}^{\text{c}}$ (eV)	λ_{max} (nm)	λ_{onset} (nm)	E_g^{d} (eV)	$E_{\text{LUMO}}^{\text{c}}$ (eV)		
PA	609	654	1.90	−3.83	621	670	1.85	−3.87	0.92	−5.72
PB	628	660	1.88	−3.75	626	659	1.88	−3.74	0.83	−5.63
PC	562	659	1.88	−3.59	559	659	1.88	−3.59	0.68	−5.48
PD	367	664	1.87	−3.74	371	662	1.87	−3.74	0.81	−5.61

^a In CHCl_3 .

^b Solution optical bandgap.

^c Calculated from optical bandgap and electrochemically obtained HOMO energy.

^d Thin film optical bandgap.

^e Potentials (vs Fc/Fc^+).

^f Solution electrochemical bandgap.

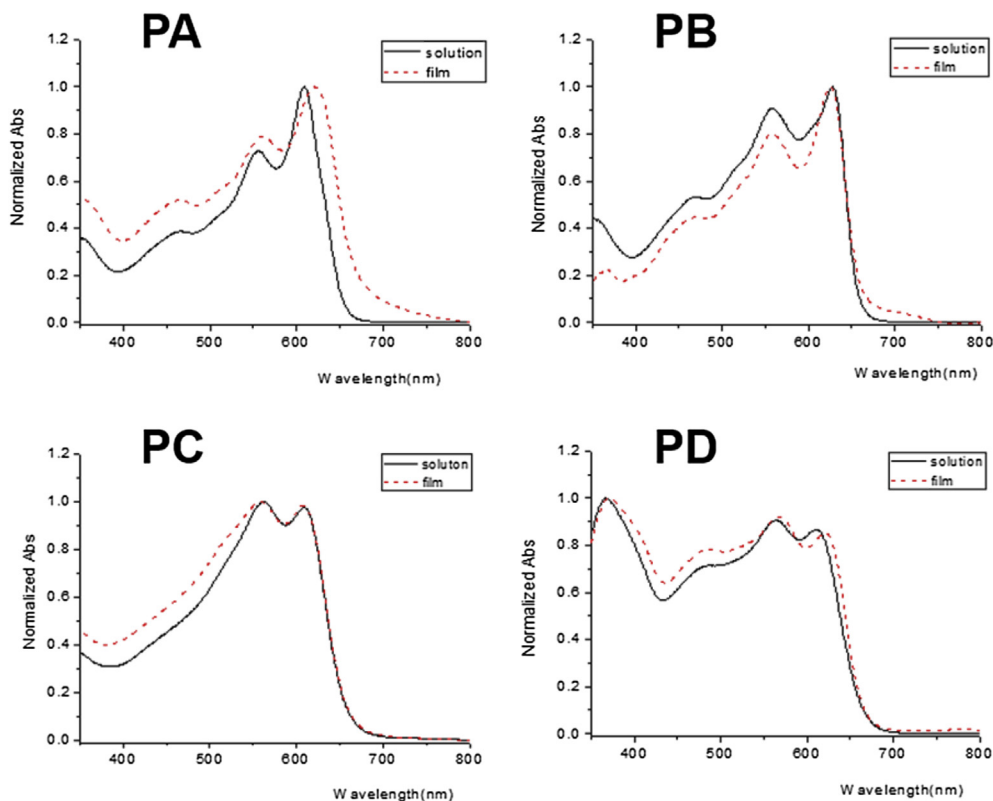


Fig. 3. Absorption spectra of **PA**, **PB**, **PC**, and **PD** in chloroform solution and as thin films.

3.4. Theoretical calculations

Theoretical calculations were performed to predict the energies and distribution of the frontier molecular orbitals by density functional theory (DFT) using the Gaussian 09 program at the B3LYP/6-31G+(d) level in the gas phase [26]. The optimized molecular geometries were confirmed to be the minimum-energy conformations by computing vibrational frequencies at the same level. To reduce the time and cost of calculation, long alkyl chains were replaced by methyl group, and the polymers were simplified to dimer. The molecular geometries of the dimers for optimization process were referred from those reported in the literature [16,27] and optimization was carried out starting from the planar structure of the dimer only. The optimized molecular geometries and frontier molecular orbitals are shown in Fig. 5, indicating that the HOMO surfaces of **PA** and **PB** are well delocalized along its backbone and

partially delocalized on the side chains. However, the HOMO surfaces of **PD** are well delocalized along both its backbone and side chains. One of the reasons that π -orbitals of the side chains on **PA** and **PB** are partially delocalized can be found that their torsional angles to the polymer backbone are as much twisted as 47.20° and 52.75° for **PA** and **PC**, respectively, indicating that the π -orbitals of the backbone and the side chains may not overlap effectively for the delocalization, because of highly twisted torsional angles. This phenomenon is also found in the previous studies [27,28] and may attribute to the poor absorption in the shorter wavelength of the UV–vis spectra of these BDTT polymers even if they have two-dimensional structures. However, the torsional angle to the polymer backbone for **PD** was calculated as 0.76° , indicating that the side chain is coplaner with its polymer backbone. As shown in Fig. 3 (**PD**), the electrons in the side chains and BDT unit are well delocalized, and this may attribute to significantly enhanced absorption

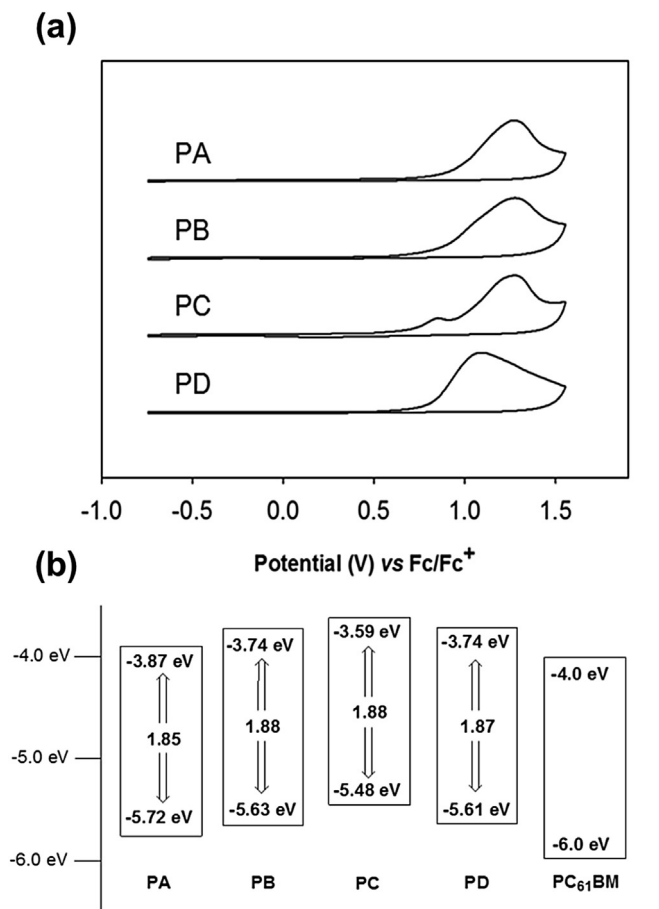


Fig. 4. (a) Cyclic voltammograms of the drop casted polymers (PA–PD) on Pt disk electrode in the presence of 100 mM TBAPF₆ in Acetonitrile at a scan rate of 100 mV/s, the potential is referenced to the Fc/Fc⁺, (b) HOMO and LUMO energy level diagram of the polymers and PC₆₁BM.

in the shorter wavelength of the UV–vis spectra of **PD**. In addition, the torsional angles between BDT and TPD units of the polymers are 12.37 and 1.14° for **PA** and **PD**, respectively, whereas that of between BDT and thiophene units of the polymers is 10.49° for **PC**. These data indicate that the polymer backbones are not much deviated from the planar conformation, and the π -orbitals of the backbone can be well delocalized by effective overlapping.

3.5. Photovoltaic properties

PSC devices were fabricated to evaluate and compare the photovoltaic properties of three differently engineered polymers by utilizing a conventional BHJ device structure of ITO/PEDOT:PSS/polymer:PC₆₁BM/LiF/Al, where PC₆₁BM was used as the electron acceptor. The device fabrication process was optimized by fine adjustment of solvents, polymer:fullerene ratios, and additives. For PSC device fabrication, various solvents such as chloroform, chlorobenzene, *o*-dichlorobenzene were screened, and chloroform was chosen as the processing solvent owing to its good solubility for polymers and wide variety of uses. However, **PB** was excluded in device fabrication, because the best solvent for its fabrication could not be obtained in spite of the scans of various solvents. Then, different polymer:fullerene (D/A) weight ratios were scanned, and the optimized weight ratios of the polymer and PC₆₁BM were determined to be 1:1, 1.5, and 1:1 for **PA**, **PC**, and **PD**, respectively, at a polymer concentration of 10 mg/mL (1 wt%) using chloroform as

the solvent. The current density–voltage (J – V) curves of the devices with photovoltaic parameters such as J_{sc} , V_{oc} , FF, and PCE, for the optimization processes based on the polymer:PC₆₁BM ratios were collected and are provided in Figs. S1–S12. The best devices from the three polymers, **PA**, **PC**, and **PD**, fabricated from chloroform without any additives showed the PCE values of 2.91%, 2.58%, and 1.71%, respectively (see Figs. S1, S5, and S9). 1,8-Diiodooctane (DIO) has been proven as an efficient and universal additive to improve the morphology of polymers [29,30]. The introduction of an optimal amount of DIO into the polymer:PC₆₁BM blends significantly enhanced the device performance. The J – V characteristics of some representative PSCs based on **PA**, **PB**, and **PD** with different amounts of DIO additive measured under simulated AM 1.5 G illumination (100 mW cm⁻²) are presented in Fig. 6a, and the devices' photovoltaic parameters, J_{sc} , V_{oc} , FF, and PCE are listed in Table 3. The optimum amounts of additive to the blend solutions were determined as 1.0%, 0.5%, and 1.0% for **PA**:PC₆₁BM, **PC**:PC₆₁BM, and **PD**:PC₆₁BM respectively. For the J – V curves of the device incorporating **PC**:PC₆₁BM as shown in Fig. 6a, the maximal device performance was achieved upon only 0.5% addition of DIO to the polymer blends and did not significantly change by adding more additive. This result suggests that **PC** tends to easily transform into its optimal geometric microstructure even with a small amount of additive, because the torsional energy between the donor and acceptor units is significantly lowered by placing the spacer to form the polymer backbone to be more planar for effective intermolecular π – π interactions. After the optimization, the PCEs of the devices significantly improved to 5.36%, 4.62%, and 2.74% for **PA**, **PC**, and **PD**, respectively. Notably, the addition of DIO to the polymer:PC₆₁BM blends significantly enhanced both the FF and J_{sc} , but only slightly improved the V_{oc} . The device fabricated from **PA** showed the optimum PCE of 5.36% benefited by high V_{oc} (>1 V) and is comparable to the optimum PCE (6.17%, PBTD-T8-TPD: PC₆₁BM) reported previously [16]. A high V_{oc} observed in this device is well in accordance with that reported previously and can be expected from the low-lying HOMO energy level of **PA** (–5.72 eV). As shown in Fig. 6b and Table 3, the device fabricated from **PC** showed the best of PCE (4.62%), which is lower than that from **PA**, mainly because of the decreased V_{oc} (0.87 V). Concerning the role of spacer in the polymer, Leclerc and others reported that the copolymers with unsubstituted thiophene spacers tend to have a low PCE value (less than 1%), because of the bad morphology of the active layer [31]. However, we found that the morphology of the polymer **PC** with unsubstituted thiophene spacers can be improved with the choice of proper alkyl chain on the BDT unit, and the addition of proper additive (see the AFM results) dramatically improved the PCE up to 4.62% from the **PC** based device. Moreover, less amount of additive (0.5% of DIO) can be used with the polymer with spacers and is desirable for long term-stability of the device. This phenomenon indicates that the introduction of spacer group may eliminate the torsional angle strain of the backbone by moving apart the neighboring alkyl chains, helping the polymer backbone to be more planar for more efficient polymer π – π stacking. Finally, we turned our attention to **PD** polymer equipped with an extended conjugated side chain on the BDT unit. The device fabricated from **PD**/PC₆₁BM (1:1) blend with 1% DIO showed the optimum PCE of 2.74% with a V_{oc} , J_{sc} , and FF of 0.98 V, 6.34 mA/cm², and 44.03%, respectively. The PCE of 2.74% appears to be much lower than those obtained from **PA** and **PC**, mainly because of much decreased J_{sc} and FF. This low PCE can be attributed from the deteriorated polymer morphology, probably because of the low solubility and low molecular weight of **PD**.

External quantum efficiency (EQE) spectra of the devices by varying the amount of DIO were measured to evaluate the photo-responses of the polymers and further confirm the accuracy of the

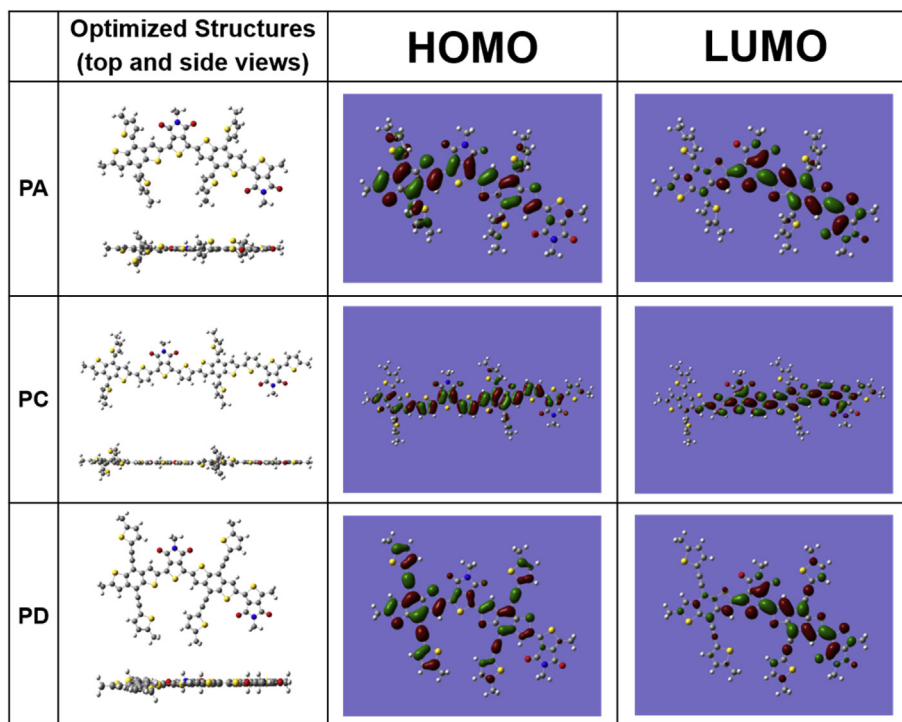


Fig. 5. Optimized molecular structures and frontier molecular orbitals of the dimers for PA, PC, and PD.

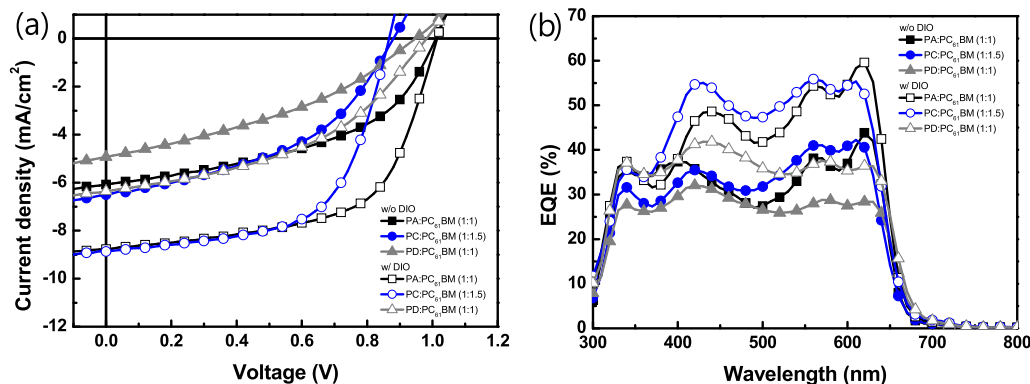


Fig. 6. (a) Current density–voltage (J – V) curves and (b) EQE curves of the PSCs based on polymer:PC₆₁BM blend without DIO (closed symbols) and with DIO (open symbols).

Table 3

Photovoltaic properties of PSCs based on polymer:PC₆₁BM blend without DIO and with DIO.

Blend	DIO	V_{oc} (V)	J_{sc} (mA/cm ²)	FF (%)	PCE (%)
PA:PC ₆₁ BM (1:1)	Without	1.01	6.08	47.43	2.91
	With 1%	1.01	8.74	60.48	5.36
PC:PC ₆₁ BM (1:1.5)	Without	0.88	6.50	45.07	2.58
	With 0.5%	0.87	8.85	60.29	4.62
PD:PC ₆₁ BM (1:1)	Without	0.95	4.93	36.68	1.71
	With 1%	0.98	6.34	44.03	2.74

photovoltaic measurements. Fig. 6b shows the EQE curves of the PSCs based on PA:PC₆₁BM (1:1), PC:PC₆₁BM (1:1.5), and PD:PC₆₁BM (1:1) by varying the amount of DIO. The EQE curves of the devices exhibited broad spectral responses ranging from 300 to 700 nm, strongly correlating with their absorption spectra (Fig. 3). The device from the optimized PA:PC₆₁BM blend with 1% DIO showed a

relatively high photo-to-current conversion efficiency over the wavelength range 340–650 nm, with monochromatic EQE values in the range ~40–60%. The device from the optimized PC:PC₆₁BM blend with 0.5% DIO showed a similar EQE curve as that from the PA blend. As shown in Fig. 7c, the device from the optimized PD:PC₆₁BM blend with 1% DIO showed relatively low photo-conversion efficiency over the entire wavelength range in comparison with those from PA and PC, with the EQE values in the range ~38–45%. Although the device incorporating PD showed low EQE values, likely attributed to its lower J_{sc} value, the EQE values were more evenly distributed over the entire wavelength range and can be understood from its absorption spectrum.

3.6. Morphology study by AFM

Atomic force microscopy (AFM) was used to further characterize the surface morphology and phase separation of the polymer:PC₆₁BM blend films to investigate the relationship between

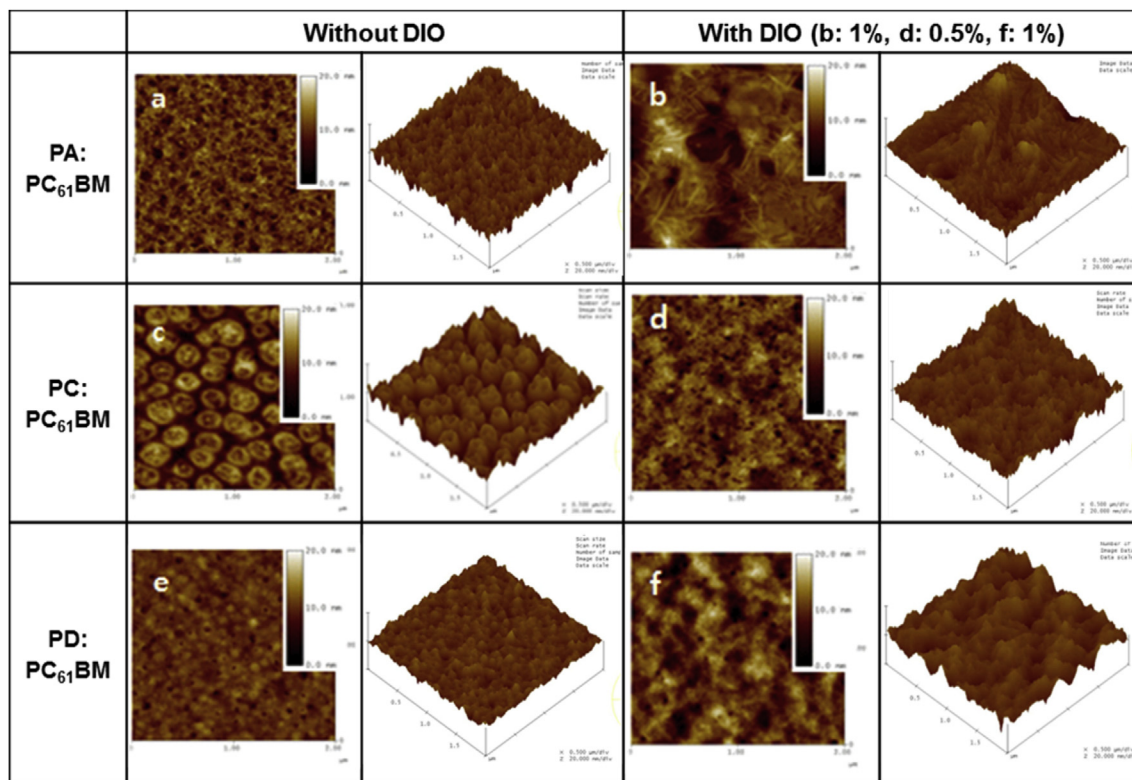


Fig. 7. Tapping-mode AFM images: topography images of the blend films of **PA**: PC₆₁BM (a), **PC**: PC₆₁BM (c), and **PD**: PC₆₁BM (e) without DIO (left) and the blend films of **PA**: PC₆₁BM (b, 1.0%), **PC**: PC₆₁BM (d, 0.5%), and **PD**: PC₆₁BM (f, 1.0%) with DIO (right).

the morphology and the photovoltaic characteristics of the devices. DIO as an additive is believed to allow a slower crystallization process during spin-coating, thus improving morphology through enhanced intermolecular ordering and well-developed phase separation. Fig. 7 shows the AFM images of the surface morphologies of the each solar cell device without and with DIO. As shown in Fig. 7(a, c, and e), the root-mean-square roughness (rms) of the blend films of **PA**:PC₆₁BM, **PC**:PC₆₁BM, and **PD**:PC₆₁BM without DIO were 2.0, 2.7, 1.2 nm, respectively. In Fig. 7(a), the nanofibril structure was observed in **PA**:PC₆₁BM film indicating a crystallinity of **PA** polymer with (100) and (010) peaks as shown in Fig. 8. The

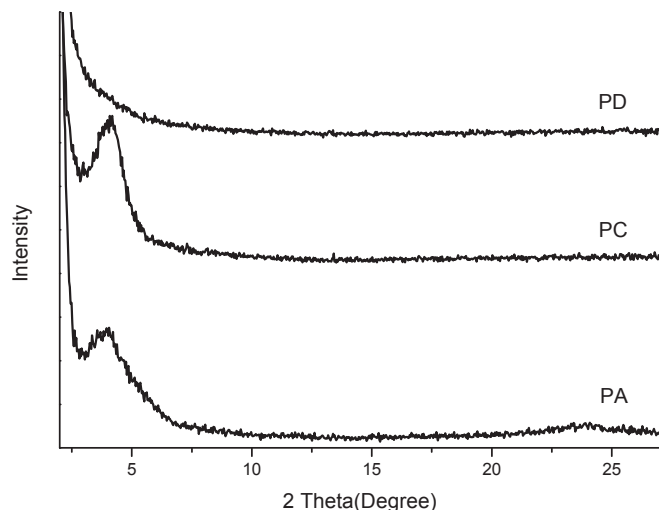


Fig. 8. XRD patterns of **PA**, **PC**, and **PD** films.

nanofibril structure with a high crystallinity is help to achieve high performance by improving charge transport in organic solar cells [34]. As shown in the images in Fig. 7c, although the blend film of **PC**:PC₆₁BM shows regularly aggregated domains (~250 nm) like tulip buttons, which is distinct morphological features compared to the other two films, the J_{sc} of **PC**:PC₆₁BM device has a higher value than those of other devices, because of the high absorption property of **PC** polymer in the range 350–600 nm. **PD**:PC₆₁BM film showed smaller granular domain size (~100 nm) than that of **PC**:PC₆₁BM film, however, this device shows a lower J_{sc} and FF than those of other polymers due to the amorphous nature (Fig. 6) and low molecular weight (Table 1) of **PD** polymer, which is mainly affected in charge transport and light absorption [35,36]. When an additive was added into the blends of polymer:PC₆₁BM, the surface roughness decreased to 1.8 and 2.3 for **PA**:PC₆₁BM and **PC**:PC₆₁BM, respectively, as evidenced by significantly improved PCEs of the devices fabricated from those blends. Unusually, the surface roughness of **PD**:PC₆₁BM blend with DIO increased from 1.2 to 2.7 despite of some improvement in the photovoltaic performance. To our surprise, the morphology of the blend of **PA**:PC₆₁BM incorporated with DIO exhibited better crystalline properties, as shown in the blend film of **PA**:PC₆₁BM with DIO (Fig. 7b). Recently, Cho and coworkers reported that BHJ-PSCs composed of highly crystalline polymer nanowires (PNWs) yielded an outstanding improvement in the PCE compared to the PCE of a device prepared without nanowires [32,33]. They also mentioned that only a few polymers formed crystalline polymer nanowires (PNWs) in the processing of the blend film. Therefore, we believe that this polymer would be a promising candidate as a polymer to be processed as crystalline polymer nanowires (PNWs). In **PC**:PC₆₁BM and **PD**:PC₆₁BM films, the additive contributed to forming distinct nanoscale phase separation by removing the grain boundary, thus increasing the J_{sc} and

FF, because of the improvement in the charge generation and transport in the active layer [29,30].

3.7. XRD analysis

The film microstructures and polymer chain packing of **PA**, **PC**, and **PD** were investigated by X-ray diffraction (XRD) measurement. Fig. 8 shows the XRD patterns of the three polymers cast from their chloroform solutions. The ordered lamellar packing ((100) plane) was observed at $2\theta = 4.05$ and 4.09° for **PA** and **PC** polymers, respectively. This peak is related to the length of the side chains of **PA** and **PC** polymers, and the distance corresponding to the lamellar spacing in the plane is smaller for **PA** ($d = 21.78$) than for **PC** ($d = 21.61$). **PA** film also has a broad peak at $2\theta = 24.1$, suggesting that the π - π stacking of (010) plane is beneficial for better charge transport in the **PA** polymer based device. **PD** film is amorphous, because of the absence of peaks in the XRD pattern. Consequently, **PA** polymer has a better crystalline structure, resulting in a better device performance compared to **PC** and **PD** polymers.

4. Conclusions

In summary, four BDT-TPD polymers were prepared by modifying alkylthienyl chains, placing a spacer group, and installing extended conjugated side chains to investigate the correlation between the structure and photovoltaic performance for these polymers. All the polymers showed high thermal stabilities, broad absorption spectra, and noticeably enhanced absorption in the entire wavelength for **PD**, because of the extended conjugated side chains. The DFT calculations reveal that the alkylthienyl side chains of **PA** and **PC** are quite twisted against the polymer backbone, whereas the side chains of **PD** are planarly aligned with the backbone, playing a critical role to the absorption patterns and intermolecular interactions. The HOMO levels of the polymers were calculated and ranged from -5.72 to -5.48 eV, indicating very low-lying HOMO energy levels. The optimized experiments on the solar cell devices based on **PA**, **PC**, and **PD** demonstrate the PCEs of 5.36, 4.62, and 2.74% respectively, with high V_{oc} from 0.87 to 1.02 V. Unlike the results reported previously, placing unsubstituted thiophene as a spacer into the polymer did not show any adverse effect on the morphology, but improved J_{sc} and reduced the amount of additive, as evidenced by a high PCE of 4.62% of the device fabricated from **PC:PC₆₁BM** with 0.5% DIO. Especially, the PSC device fabricated from **PD** bearing extended conjugated side chains showed a low PCE of 2.74%, mainly because of the deteriorated morphological characteristics. However, **PD** has promising properties in the noticeably broad range of absorption and strong intermolecular π - π stacking, which may provide valuable guidelines to design and improve BDT based D-A polymers for high efficiency polymer solar cells.

Acknowledgements

This work was supported by NRF-2012R1A1A2042473.

Appendix A. Supplementary data

Supplementary data related to this article can be found at <http://dx.doi.org/10.1016/j.orgel.2016.05.007>.

References

- [1] F.C. Krebs, S.A. Gevorgyan, J. Alstrup, A roll-to-roll process to flexible polymer solar cells: model studies, manufacture and operational stability studies, *J. Mater. Chem.* 19 (2009) 5442–5451.
- [2] F.C. Krebs, T.D. Nielsen, J. Fyenbo, M. Wadström, M.S. Pedersen, Manufacture, integration and demonstration of polymer solar cells in a lamp for the "Lighting Africa" initiative, *Energy Environ. Sci.* 3 (2010) 512–525.
- [3] B. Azzopardi, C.J. Emmott, A. Urbina, F.C. Krebs, J. Mutale, J. Nelson, Economic assessment of solar electricity production from organic-based photovoltaic modules in a domestic environment, *Energy Environ. Sci.* 4 (2011) 3741–3753.
- [4] N. Espinosa, M. Hösel, D. Angmo, F.C. Krebs, Solar cells with one-day energy payback for the factories of the future, *Energy Environ. Sci.* 5 (2012) 5117–5132.
- [5] K.G. Jespersen, W.J. Beenken, Y. Zaushtsyn, A. Yartsev, M. Andersson, T. Pullerits, V. Sundström, The electronic states of polyfluorene copolymers with alternating donor-acceptor units, *J. Chem. Phys.* 121 (2004) 12613–12617.
- [6] E. Perzon, F. Zhang, M. Andersson, W. Mammo, O. Inganäs, M.R. Andersson, A conjugated polymer for near infrared optoelectronic applications, *Adv. Mater.* 19 (2007) 3308–3311.
- [7] A. Gadisa, W. Mammo, L.M. Andersson, S. Admassie, F. Zhang, M.R. Andersson, O. Inganäs, A new donor-acceptor-donor polyfluorene copolymer with balanced electron and hole mobility, *Adv. Funct. Mater.* 17 (2007) 3836–3842.
- [8] M. Zhang, X. Guo, Y. Li, Photovoltaic performance improvement of D-A copolymers containing bithiazole acceptor unit by using bithiophene bridges, *Macromolecules* 44 (2011) 8798–8804.
- [9] Y. Huang, X. Guo, F. Liu, L. Huo, Y. Chen, T.P. Russell, C.C. Han, Y. Li, J. Hou, Improving the ordering and photovoltaic properties by extending π -conjugated area of electron-donating units in polymers with D-A structure, *Adv. Mater.* 24 (2012) 3383–3389.
- [10] E. Zhou, J. Cong, K. Hashimoto, K. Tajima, Introduction of a conjugated side chain as an effective approach to improving donor-acceptor photovoltaic polymers, *Energy Environ. Sci.* 5 (2012) 9756–9759.
- [11] G. Zhang, Y. Fu, Q. Zhang, Z. Xie, Benzo [1, 2-b: 4, 5-b'] dithiophene-dioxypyrrolothiophene copolymers for high performance solar cells, *Chem. Commun.* 46 (2010) 4997–4999.
- [12] Y. Zhang, S.K. Hau, H.-L. Yip, Y. Sun, O. Acton, A.K.-Y. Jen, Efficient polymer solar cells based on the copolymers of benzodithiophene and thienopyrroledione, *Chem. Mater.* 22 (2010) 2696–2698.
- [13] Y. Zou, A. Najari, P. Berrouard, S. Beaupré, B. Reida Aïch, Y. Tao, M. Leclerc, A thieno [3, 4-c] pyrrole-4, 6-dione-based copolymer for efficient solar cells, *J. Am. Chem. Soc.* 132 (2010) 5330–5331.
- [14] C. Piliago, T.W. Holcombe, J.D. Douglas, C.H. Woo, P.M. Beaujuge, J.M. Fréchet, Synthetic control of structural order in N-alkylthieno [3, 4-c] pyrrole-4, 6-dione-based polymers for efficient solar cells, *J. Am. Chem. Soc.* 132 (2010) 7595–7597.
- [15] K. Lu, J. Fang, Z. Yu, H. Yan, X. Zhu, Y. Zhang, C. He, Z. Wei, Improving the performance of polymer solar cells by altering polymer side chains and optimizing film morphologies, *Org. Electron.* 13 (2012) 3234–3243.
- [16] J. Yuan, Z. Zhai, H. Dong, J. Li, Z. Jiang, Y. Li, W. Ma, Efficient polymer solar cells with a high open circuit voltage of 1 volt, *Adv. Funct. Mater.* 23 (2013) 885–892.
- [17] K. Lu, J. Fang, H. Yan, X. Zhu, Y. Yi, Z. Wei, A facile strategy to enhance absorption coefficient and photovoltaic performance of two-dimensional benzo [1, 2-b: 4, 5-b'] dithiophene and thieno [3, 4-c] pyrrole-4, 6-dione polymers via subtle chemical structure variations, *Org. Electron.* 14 (2013) 2652–2661.
- [18] H.-S. Chung, W.-H. Lee, C.E. Song, Y. Shin, J. Kim, S.K. Lee, W.S. Shin, S.-J. Moon, I.-N. Kang, Highly conjugated side-chain-substituted benzo [1, 2-b: 4, 5-b'] dithiophene-based conjugated polymers for use in polymer solar cells, *Macromolecules* 47 (2013) 97–105.
- [19] J.-H. Kim, C.E. Song, B. Kim, I.-N. Kang, W.S. Shin, D.-H. Hwang, Thieno [3, 2-b] thiophene-substituted benzo [1, 2-b: 4, 5-b'] dithiophene as a promising building block for low bandgap semiconducting polymers for high-performance single and tandem organic photovoltaic cells, *Chem. Mater.* 26 (2014) 1234–1242.
- [20] H. Yao, H. Zhang, L. Ye, W. Zhao, S. Zhang, J. Hou, Molecular design and application of a photovoltaic polymer with improved optical properties and molecular energy levels, *Macromolecules* 48 (2015) 3493–3499.
- [21] J. Hou, M.-H. Park, S. Zhang, Y. Yao, L.-M. Chen, J.-H. Li, Y. Yang, Bandgap and molecular energy level control of conjugated polymer photovoltaic materials based on benzo [1, 2-b: 4, 5-b'] dithiophene, *Macromolecules* 41 (2008) 6012–6018.
- [22] P. Sista, B. Xue, M. Wilson, N. Holmes, R.S. Kularatne, H. Nguyen, P.C. Dastoor, W. Belcher, K. Poole, B.G. Janesko, Influence of the alkyl substituents spacing on the solar cell performance of benzodithiophene semiconducting polymers, *Macromolecules* 45 (2012) 772–780.
- [23] J.-H. Kim, H.U. Kim, I.-N. Kang, S.K. Lee, S.-J. Moon, W.S. Shin, D.-H. Hwang, Incorporation of pyrene units to improve hole mobility in conjugated polymers for organic solar cells, *Macromolecules* 45 (2012) 8628–8638.
- [24] J.-M. Jiang, H.-K. Lin, Y.-C. Lin, H.-C. Chen, S.-C. Lan, C.-K. Chang, K.-H. Wei, Side chain structure affects the photovoltaic performance of two-dimensional conjugated polymers, *Macromolecules* 47 (2013) 70–78.
- [25] J.-L. Bredas, Mind the gap!, *Mater. Horiz.* 1 (2014) 17–19.
- [26] M. Frisch, G. Trucks, H. Schlegel, G. Scuseria, M. Robb, J. Cheeseman, G. Scalmani, V. Barone, B. Mennucci, G. Petersson, H. Nakatsuji, M. Caricato, X. Li, H. Hratchian, A. Izmaylov, J. Bloino, G. Zheng, J. Sonnenberg, M. Hada, M. Ehara, K. Toyota, R. Fukuda, J. Hasegawa, M. Ishida, T. Nakajima, Y. Honda, O. Kitao, H. Nakai, T. Vreven, J. Montgomery, J. Peralta, F. Ogliaro, M. Bearpark,

- J. Heyd, E. Brothers, K. Kudin, V. Staroverov, R. Kobayashi, J. Normand, K. Raghavachari, A. Rendell, J. Burant, S. Iyengar, J. Tomasi, M. Cossi, N. Rega, J. Millam, M. Klene, J. Knox, J. Cross, V. Bakken, C. Adamo, J. Jaramillo, R. Gomperts, R. Stratmann, O. Yazyev, A. Austin, R. Cammi, C. Pomelli, J.W. Ochterski, R. Martin, K. Morokuma, V. Zakrzewski, G. Voth, P. Salvador, J. Dannenberg, S. Dapprich, A. Daniels, Ö. Farkas, J. Foresman, J. Ortiz, J. Cioslowski, D. Fox, 09, Revision A.02, Gaussian, Inc., Wallingford, CT, 2009.
- [27] J. Warnan, A. El Labban, C. Cabanetos, E.T. Hoke, P.K. Shukla, C. Risko, J.-L. Bredas, M.D. McGehee, P.M. Beaujuge, Ring substituents mediate the morphology of PBDTTPD-PCBM bulk-heterojunction solar cells, *Chem. Mater.* 26 (2014) 2299–2306.
- [28] S. Zhang, L. Ye, W. Zhao, D. Liu, H. Yao, J. Hou, Side chain selection for designing highly efficient photovoltaic polymers with 2D-conjugated structure, *Macromolecules* 47 (2014) 4653–4659.
- [29] J.K. Lee, W.L. Ma, C.J. Brabec, J. Yuen, J.S. Moon, J.Y. Kim, K. Lee, G.C. Bazan, A.J. Heeger, Processing additives for improved efficiency from bulk heterojunction solar cells, *J. Am. Chem. Soc.* 130 (2008) 3619–3623.
- [30] S.J. Lou, J.M. Szarko, T. Xu, L. Yu, T.J. Marks, L.X. Chen, Effects of additives on the morphology of solution phase aggregates formed by active layer components of high-efficiency organic solar cells, *J. Am. Chem. Soc.* 133 (2011) 20661–20663.
- [31] A. Najari, S. Beaupré, P. Berrouard, Y. Zou, J.R. Pouliot, C. Lepage-Pérusse, M. Leclerc, Synthesis and characterization of new thieno [3, 4-c] pyrrole-4, 6-dione derivatives for photovoltaic applications, *Adv. Funct. Mater.* 21 (2011) 718–728.
- [32] J. Lee, S.B. Jo, M. Kim, H.G. Kim, J. Shin, H. Kim, K. Cho, Donor–acceptor alternating copolymer nanowires for highly efficient organic solar cells, *Adv. Mater.* 26 (2014) 6706–6714.
- [33] J.-H. Kim, M. Kim, H. Jinnai, T.J. Shin, H. Kim, J.H. Park, S.B. Jo, K. Cho, Organic solar cells based on three-dimensionally percolated polythiophene nanowires with enhanced charge transport, *ACS Appl. Mater. Interfaces* 6 (2014) 5640–5650.
- [34] J.-H. Kim, J.B. Park, I.H. Jung, A.C. Grimsdale, S.C. Yoon, H. Yang, D.-H. Hwang, Well-controlled thieno[3,4-c]pyrrole-4,6-(5H)-dione based conjugated polymers for high performance organic photovoltaic cells with the power conversion efficiency exceeding 9%, *Energy Environ. Sci.* 8 (2015) 2352–2356.
- [35] J. Subbiah, B. Purushothaman, M. Chen, T. Qin, M. Gao, D. Vak, F.H. Scholes, X. Chen, S.E. Watkins, G.J. Wilson, A.B. Holmes, W.W. Wong, D.J. Jones, Organic solar cells using a high-molecular-weight benzodithiophene-benzothiadiazole copolymer with an efficiency of 9.4%, *Adv. Mater.* 27 (2015) 702–705.
- [36] S. Wakim, S. Beaupre, N. Blouin, B.R. Aich, S. Rodman, R. Gaudiana, Y. Tao, M. Leclerc, Highly efficient organic solar cells based on a poly(2,7-carbazole) derivative, *J. Mater. Chem.* 19 (2009) 5351–5358.